Contributors to Future Stratospheric Climate Change: An Idealized Chemistry–Climate Model Sensitivity Study

M. M. Hurwitz [1, 2], **P. Braesicke** [1] and **J. A. Pyle** [1]

1 **Centre for Atmospheric Science and NCAS–Climate, University of Cambridge, Cambridge, UK**

2 **Now at: NASA Postdoctoral Program, NASA Goddard Space Flight Center, Greenbelt, MD, USA**

Corresponding author information

Email address: **margaret.m.hurwitz@nasa.gov**

Mailing address: **NASA Goddard Space Flight Center**
Code 613.3
Greenbelt, MD
USA 20771

Abstract

Within the framework of an idealized model sensitivity study, three of the main contributors to future stratospheric climate change are evaluated: increases in greenhouse gas concentrations, ozone recovery, and changing sea surface temperatures (SSTs). These three contributors are explored in combination and separately, to test the interactions between ozone and climate; the linearity of their contributions to stratospheric climate change is also assessed.

In a simplified chemistry–climate model, stratospheric global mean temperature is most sensitive to CO_2 doubling, followed by ozone depletion, then by increased SSTs. At polar latitudes, the Northern Hemisphere (NH) stratosphere is more sensitive to changes in CO_2, SSTs and O_3 than is the Southern Hemisphere (SH); the opposing responses to ozone depletion under low or high background CO_2 concentrations, as seen with present–day SSTs, are much weaker and are not statistically significant under enhanced SSTs. Consistent with previous studies, the strength of the Brewer–Dobson circulation is found to increase in an idealized future climate; SSTs contribute most to this increase in the upper troposphere/lower stratosphere (UT/LS) region, while CO_2 and ozone changes contribute most in the stratosphere and mesosphere.

1 Motivations

Braesicke et al., 2006; hereafter BHP2006) examined the stratospheric sensitivity to ozone depletion and to the doubling of CO_2. Their study used a sea surface temperature (SST) climatology with a repeating annual cycle, representative of the late 20th century. That is, SSTs did not increase in response to increased greenhouse gas concentrations; their experiments primarily examined the stratospheric radiative impact of increased CO_2.

Using the same simplified chemistry–climate model (CCM) as in BHP2006, the relative response to changes in CO_2 and O_3 concentrations and sea surface temperatures (SSTs) is explored; this approach considers the combined stratospheric response to warming from both the troposphere and the upper ocean by prescribing 'future' SSTs. To separate the three proposed contributions to stratospheric climate change, global mean temperature, eddy heat flux, winds and ozone are diagnosed in each of a set of idealized time–slice experiments. The strength of the Brewer-Dobson circulation, and the connection between tropical upwelling and polar ozone in an idealized present–day climate scenario is compared with an idealized future climate.

BHP2006 found that global mean temperatures cooled in response to both an O_3 change (2000–like – 1980–like) and a CO_2 change (704ppmv – 352ppmv), throughout the middle atmosphere. However, neither change much affected tropospheric temperatures because the same SST climatology was prescribed in all experiments. Recent trends in observed SSTs, as well as coupled ocean–atmosphere simulations of the 21st century, suggest that anthropogenic climate change will continue to affect the temperature of the sea surface (i.e. Johns et al., 2003). When 'future' SSTs are used in conjunction with a doubled–CO_2 atmosphere, the troposphere should respond by warming more significantly than for a doubling of CO_2 alone. Also, there may be feedbacks between

these increased tropospheric temperatures and global mean temperature in the stratosphere that can be considered when CO_2 concentrations and SSTs are increased together.

BHP2006 showed that two dynamical relationships held for a set of four idealized climate change simulations in a simplified CCM. First, the negative correlation between zonal mean zonal wind (a proxy for polar vortex strength) and total O_3 at Northern Hemisphere (NH) high latitudes in January, as was originally discussed by Braesicke and Pyle (2004). Second, high–latitude temperature was seen to mimic changes in mid-latitude heat flux (the 'tropospheric forcing' by planetary waves) in the December–January–February (DJF) season (e.g., as shown by Newman et al., 2001). This paper will address how warmer SSTs affect the character of these two relationships.

In the time–slice experiments with present–day SSTs evaluated by BHP2006, it was noted that the behavior of the NH polar vortex (and thus of polar ozone) depended on the background CO_2 concentration: The single–CO_2 experiments responded to ozone depletion in the opposite sense to the doubled CO_2 experiments; this effect provided an example of the competition between radiative and dynamical processes in the polar stratosphere. This paper will determine whether increased SSTs enhance cooling in the middle atmosphere, thus favoring stronger polar vortices in all experiments. Do 'future' SSTs affect the coupling between ozone depletion and tropospheric forcing? Sections 3, 4 and 5 will assess the response of the UM chemistry–climate model to changes in O_3, CO_2 and SSTs with a set of transport, dynamical, radiative and chemical diagnostics. Section 6 will summarize the main conclusions.

2 Methods

2.1 Model Description

The following discussion refers to a set of eight time–slice integrations conducted with version 4.5.1 of the MetOffice Unified Model (UM). In this configuration, the UM has 3.75° x 2.5° horizontal resolution and 64 vertical levels, with ~1.3km resolution in the stratosphere. The climate model is coupled non-interactively with the Cariolle and Déqué (1986) parameterized stratospheric ozone chemistry scheme. The chemical module contains a cold tracer (X) used to mimic the impact of polar stratospheric clouds (PSCs) on polar ozone: when temperatures drop below a given threshold (~195K for nitric acid trihydrate at 50hPa) the cold tracer is produced exponentially with a time constant of four hours; the cold tracer decays with a ten–day time constant. This model setup has been used previously and documented by Braesicke and Pyle (2003, 2004) and Pyle et al. (2005).

2.2 Experimental Design

Eight 20–year time–slice experiments will be discussed in this paper (see Table 1). Each experiment tests the combination of one of two CO_2 concentrations ($1xCO_2$ or $2xCO_2$), stratospheric ozone climatologies (1980–like or 2000–like), and SST and sea ice climatologies (present–day or future). Differences between pairs of experiments can be examined so as to isolate the effects of changes in each of the three parameters (ozone, CO_2 and SSTs) on the climate of the middle atmosphere. Since one of the time–slice experiments represents an idealized present–day climate (1B; low CO_2, depleted ozone layer and present–day SSTs) and another represents the likely stratospheric climate in the mid– to late 21st century (2C; high CO_2, recovered ozone layer and future SSTs), the 2C–1B difference can be interpreted as the 'climate change signal' (see WMO, 2007).

A 1980–like ozone climatology is prescribed in experiment 1A, whereas a 2000–like ozone climatology, with substantial polar ozone deficits as compared with

the 1980–like climatology, is prescribed in experiment 1B. Experiments 1A and 1B use a background CO_2 concentration of 352ppmv. Experiments 2A and 2B are designed to investigate the same change under doubled CO_2 (704ppmv) conditions. As discussed by BHP2006, annually repeating boundary conditions are imposed in all four experiments: AMIP II[1] sea surface temperature (SST) and sea ice climatologies representative of the late 20th century[2]. Volcanic aerosols and the solar cycle are not considered. Experiments 1C to 2D are identical to experiments 1A to 2B, except that they use the 'future' SST climatology described in the next section. The difference in the setup between experiments 1A and 1C, for example, is solely a switch from the present–day to the future SST climatology, as is the difference between experiments 1B and 1D, 2A and 2C, and 2B and 2D.

2.3 Construction of a 'Future' SST Climatology

Including SSTs as a factor in this study, and thus examining the impact of the ocean surface on the stratospheric chemistry–climate system, requires a 'future' SST climatology. While some CCMs now include an interactive ocean model, UM 4.5.1 is an atmosphere–only model and future SSTs derived from another ocean–atmosphere model simulation must be prescribed. In the present model study, a future SST dataset is constructed by adding a twelve–month set of SST anomalies to the existing present–day SST climatology. A MetOffice SST dataset, spanning from 1970 to 2020, merges HadISST[3] data (1970–1995) with SST and sea ice output from HadGEM1 simulations (beginning in 1995). The 'climate change' SST anomalies are defined as the difference between mean SSTs in the 1970s (1971–1980) and mean SSTs the 2010s (2011–2020) from this MetOffice dataset.

148

[1] http://www-pcmdi.llnl.gov/projects/amip/AMIP2EXPDSN/BCS_OBS/amip2_bcs.htm.

[2] The 'present–day' SST and sea ice climatologies were defined as the AMIP II 1979-1996 mean.

[3] http://hadobs.metoffice.com/hadisst.

The 2010s – 1970s differences are large enough to simulate differences between present–day SSTs and those projected for the mid–21st century, and thus provide a stratospheric response.

The idealized 'climate change' SST anomalies (i.e. future – present–day) are generally positive. In the tropics and at mid–latitudes, anomalies are of the order of 1–2K (consistent with coupled ocean–atmosphere predictions of SST changes by the mid–21st century; see IPCC, 2007). The largest positive differences occur at high latitudes. Near the Gulfstream and Kuroshio currents, the SST changes exceed 10K; this is larger than predicted by most ocean–atmosphere models (IPCC, 2007). In the tropical Pacific Ocean, the climate change anomalies are positive but small (up to 1.5K) in the Intertropical Convergence Zone (ITCZ), and negligible or slightly negative to the north and south of this region. The strongest positive–negative–positive pattern occurs in the DJF season; this is the pattern of SST anomalies that defines El Niño events. There is a positive trend in the 1970–2020 timeseries of HadGEM1 SSTs in the Niño 3.4[4] region. This finding is in agreement with Timmermann et al. (1999), who predict a climate change–induced shift toward an increasingly positive Niño 3.4 index, and thus toward more frequent El Niño events, in future.

3 Radiative and Dynamical Response to Changes in Ozone, CO_2 and SSTs

3.1 Global Mean Temperature

Profiles of global and annual mean temperature differences allow for an easy assessment of overall radiative changes, suppressing dynamical changes (important at seasonal timescales) and their effects on the thermal structure of the atmosphere. Consistent with Shine et al. (2003, 2008), in the idealized time–

[4] Monthly mean SST anomalies from the 1950–1999 period in the 120°W–170°W, 5°S–5°N region (see Trenberth, 1997).

176 slice experiments, the middle atmosphere cools in response to both ozone
177 depletion (with a small peak in the lower stratosphere and a larger peak
178 centered at 1hPa) and increased CO_2 concentrations (with the strongest
179 cooling at the stratopause). Profiles of the four sets of responses to ozone
180 depletion (Fig. 1, left–hand panel) are indistinguishable from 1000 to 0.1hPa; the
181 responses are the same for both SST climatologies (i.e. 1B–1A ≈ 1D–1C) and for
182 both CO_2 concentrations (1B–1A ≈ 2B–2A). That is, the global mean
183 temperature response to ozone depletion is independent of both background
184 CO_2 and thermal forcing from the sea surface. Similarly, the response to
185 doubled CO_2 (Fig. 1, centre panel) is the same for both ozone climatologies (i.e.
186 2A–1A ≈ 2B–1B) and for either present–day or future SSTs (2A–1A ≈ 2C–1C).
187
188 The troposphere and lower stratosphere are warmer in the future SST
189 experiments than in the experiments using present–day SSTs (Fig. 1, right–hand
190 panel). The magnitude of the SST–related change in global mean stratospheric
191 temperature is far smaller than found for CO_2 doubling or for ozone depletion:
192 Under future SSTs, the troposphere warms as much as 1.3K, while the lower
193 stratosphere warms by ~0.25K. Similarly to the response to ozone depletion and
194 doubled CO_2, the response to the change in SSTs is similar under the differing
195 ozone and CO_2 conditions. Small differences between the four pairs of
196 experiments arise in the upper troposphere/lower stratosphere region, likely due
197 to mismatches in the thermal forcing between the prescribed SSTs and
198 atmospheric greenhouse gas concentrations.
199
200 As in the annual mean, future SSTs enhance warming in the upper
201 troposphere/lower stratosphere region and raise the level where no
202 temperature difference occurs throughout the seasonal cycle (not shown; see
203 Hurwitz, 2008). This finding agrees with previous studies (i.e. Chakrabarty et al.,

204 2001; Fomichev et al., 2007; Lorenz and DeWeaver, 2007) that have found a link
205 between climate change and tropopause height.
206
207 **3.2 Wintertime Lower Stratospheric Temperature, Eddy Heat Flux and**
208 **Geopotential Height**
209 Tropospheric forcing by planetary waves has a large influence on stratospheric
210 temperatures, particularly in winter. Previous studies (e.g., Newman et al., 2001;
211 Austin et al., 2003; Cagnazzo et al., 2006) have used the zonal mean eddy heat
212 flux at 100hPa, averaged over a mid–latitude band (40°N/S and 80°N/S) and
213 over a two–month time period, to diagnose the tropospheric forcing. Fig. 2
214 shows the modeled heat flux with respect to the 50hPa polar temperature. For
215 the NH, December–January (positive) heat flux is plotted against January–
216 February temperature, while for the SH, August–September (negative) heat flux
217 is plotted against September–October temperature. Fig. 2 shows that, for the
218 set of eight experiments, the relationship between tropospheric forcing and
219 polar temperature is linear and positive[5]: Increased tropospheric forcing in the
220 early winter leads to increased polar temperatures at higher altitudes somewhat
221 later in the winter. As expected, Southern polar temperatures are lower (by
222 roughly 20K) than are northern polar temperatures.
223
224 The slopes of the regression lines are steeper in the NH than in the Southern
225 Hemisphere (SH). The mean slope of the eight experiments is 1.29 m^{-1} s in the NH
226 and –0.80 m^{-1} s in the SH. These values are in agreement with the analysis by
227 Austin et al. (2003) that found the heat flux–temperature slopes based on the
228 National Centers for Environmental Prediction/National Center for Atmospheric
229 Research (NCEP/NCAR) reanalysis (Kalnay et al., 1996) to be 1.49 ± 0.27 m^{-1} s
230 (NH) and –0.89 ± 0.16 m^{-1} s (SH). This result suggests that the NH polar region is

230
[5] Heat flux is poleward in both hemispheres: positive (negative) values indicate northward (southward) heat flux.

231 more sensitive to changes in tropospheric forcing than is the southern polar
232 region.
233
234 For the NH winter season stronger heat fluxes and lower temperatures are found
235 in experiment 2C (idealized future climate; burgundy) relative to experiment 1B
236 (idealized present–day climate; turquoise). This result agrees with the work of
237 Manzini et al. (2003), who found a downward shift of the heat flux versus
238 temperature regression (perpendicular to the original slopes)) between 1960–like
239 and 2000–like time–slice simulations. In the UM experiments, however, the shift
240 toward stronger heat fluxes and lower temperatures is not significantly larger
241 than the signal due to interannual variability.
242
243 In contrast to the NH, the SH interannual variability is lower, and there is little
244 change in the heat flux and temperature values between the eight
245 experiments. This suggests that the dynamics of the SH stratosphere are not as
246 sensitive to changes in greenhouse gases, SSTs or ozone climatologies, though
247 SH winters are slightly cooler in the doubled–CO_2 experiments. Rather, the SH
248 polar stratosphere is closer to being in radiative equilibrium as compared with
249 the NH.
250
251 As noted by BHP2006, when present–day SSTs are prescribed, DJF heat flux
252 differences due to ozone depletion are positive in a single CO_2 atmosphere (1B–
253 1A) but negative in a doubled CO_2 atmosphere (2B–2A). These differences[6] are
254 shown in the two leftmost bars in Fig. 3. While the responses to ozone depletion
255 have the opposite sign when future SSTs are prescribed, the 1C–1D heat flux
256 difference is not statistically distinct from the 2D–2C difference. Consistent with
257 the heat flux differences described above, temperature and geopotential

257
[6] In figure 3, heat flux differences due to ozone depletion are shown as 1A–1B, 2A–2B, etc. as this clarifies the three contributions to the climate change signal, i.e. 2C–1B = (2C–2A) + (2A–1A) + (1A–1B).

height differences due to ozone depletion are small in the experiments using future SSTs (see Hurwitz, 2008).

The error bars in Fig. 3 reveal the high degree of interannual variability in tropospheric forcing during the NH winter season, and thus the difficulty in evaluating heat flux differences and their subsequent effects on stratospheric dynamics. The only heat flux differences from that are statistically different from zero are the three changes of parameter relative to experiment 1A (ozone depletion, doubling of CO_2 and increasing SSTs). While heat flux increases due to climate change (2C–1B), dynamical warming of the lower stratosphere is overwhelmed by the radiative cooling associated with doubled CO_2 and increasing SSTs. In the NH winter, 2C–1B temperature and geopotential height differences at 50hPa are generally negative (up to 3K and 30m, respectively; not shown).

4 Chemical Response to Changes in Ozone, CO_2 and SSTs

4.1 Relationship Between Polar Vortex Strength and Ozone at NH High Latitudes

The strong relationship between NH polar vortex strength and high–latitude total ozone seen in other CCM experiments (e.g., Braesicke and Pyle, 2004; BHP2006) extends to the four experiments using future SSTs. The slope of the regression line fitting each set of 20 points in experiments 1C through 2D is very similar to that seen in experiments 1A, as is the range of zonal wind and total ozone values (Fig. 4a).

Fig. 4b shows the mean regression line of all eight 20–year time–slice experiments as well as the mean zonal wind and total ozone values for each experiment. As noted by BHP2006, experiments where present–day SSTs are prescribed (1A–2B) exhibit a 'flip flop' response to ozone depletion. The means of the future SST

experiments (1C through 2D) are situated between these two states (1A/2B and 1B/2A); differences in the mean zonal winds and ozone in the future SST experiments are not statistically significant.

4.2 Polar Ozone Loss as a Function of PSC Volume

Rex et al. (2004, 2006) found a linear relationship between column ozone loss and PSC volume during the NH winter, in observations of the past two decades. BHP2006 examined this same relationship in four UM experiments using present–day SSTs (1A–2B). The strongest correlation between ozone loss and PSC volume was found in experiment 1A (1980–like ozone and $1xCO_2$; $r = 0.98$), while somewhat weaker linear relationships were found in two other experiments (1B and 2A). In experiment 2B (2000–like ozone and $2xCO_2$), ozone losses were clustered around 90DU despite interannual variation in PSC volumes and polar temperatures.

The relationship between ozone loss and PSC volume is examined in the future SST experiments (1C–2D). Just as for experiments 1A–2B, PSC volume is defined as the sum of all grid cells where cold tracer values exceed a fixed threshold (0.95). For each time–slice experiment and for each winter season, the DJF average PSC volume is then sorted into size classes (bin width $\Delta = 1 \cdot 10^7$ km^3; bin overlap $\delta = 0.5 \cdot 10^7$ km^3). Also, the modeled January mean polar temperature (at 30hPa, north of 85°N), and the wintertime column ozone loss from November to March (within the 400 to 550K potential temperature layer) are calculated for each winter and sorted according to the associated PSC volume size class. The linear relationship between ozone loss and DJF PSC volume in experiments 1C and 2D (1A and 2B with future SSTs) have slopes nearly identical to that found in 1A and a good fit ($r \sim 0.85$). Another of the future SSTs experiments (1D) has a similar slope but a lower correlation coefficient. The idealized future climate

315 scenario (2C) exhibits the same 'saturation' behavior as does experiment 2B:
316 wintertime column ozone losses do not correlate with PSC volumes.
317
318 In the NH winter, PSC volumes and polar temperatures are related by a power
319 law. The highest mean wintertime PSC volumes generally correspond with the
320 lowest mean January polar temperatures, as PSC formation is highly
321 temperature-dependent. Three of the future SST experiments have continuous
322 temperature distributions, similarly to experiment 1A (refer to BHP2006, Fig. 7).
323 The idealized future climate scenario (2C) has a bimodal distribution, as seen in
324 two of the experiments with present–day SSTs (1B and 2A).
325

326 5 Sensitivity of the Brewer–Dobson Circulation to Ozone Depletion
327 and Climate Change

328 Tropospheric forcing changes in response to ozone depletion/recovery and
329 climate change, particularly during the NH winter season, are likely to be linked
330 to changes in the strength of the Brewer–Dobson circulation (BDC; originally
331 described by Brewer (1949) and Dobson (1956)). Tropospheric forcing correlates
332 not only with stratospheric mid-winter temperatures in the lower stratosphere
333 (e.g., as shown in Fig. 2) and with polar ozone, but is also connected to the
334 residual circulation in the middle atmosphere. Newman et al. (2001) calculated
335 that a 10% reduction in the 100hPa eddy heat flux would weaken the BDC by
336 10%. Conversely, recent increases in tropospheric forcing (as discussed by
337 Dhomse et al., 2006) may have caused a strengthening of the stratospheric
338 circulation. Modeling studies by Butchart and Scaife (2001), Austin and Li (2006)
339 and Li et al. (2008) have shown that increased greenhouse gas concentrations
340 lead to a strengthened BDC in the middle atmosphere. Increased heating near
341 the equator and thus increased upward mass flux in the tropics is a key part of
342 the mechanism that links greenhouse gas concentrations with a stronger
343 Brewer–Dobson circulation (Eichelberger and Hartmann, 2005). Butchart and

Scaife (2001) and Li et al. (2008) found increased tropical upwelling in conjunction with increased downwelling at high latitudes, in climate change simulations, but could not provide an unambiguous mechanism for the strengthening. Climate change–related strengthening of the BDC has not been observed as yet (Engel et al., 2009).

The present study will separate the effects of each parameter change (ozone depletion/recovery, increased greenhouse gas concentrations and increased SSTs) on the strength and character of the BDC. This study complements a recent study by Oman et al. (2009), which examined changes in the age of stratospheric air in transient simulations of the recent past and future.

5.1 Qualitative Streamfunction Analysis

For each of the eight time–slice experiments, the residual streamfunction is calculated following Andrews et al. (1987). A latitude–height cross–section of the residual streamfunction in the idealized present–day climate simulation (1B), for the DJF season, is shown in Fig. 5a. Many features of the observed meridional circulation are reproduced: first, the separation of transport toward the South Pole (negative contours) from transport toward the North Pole (positive contours) is located just south of the equator (due to the southward shift of the ITCZ during the NH winter season). The strongest transport occurs in the troposphere; the Hadley and Ferrell cells can be seen in the tropics and at mid-latitudes, respectively, and in both hemispheres. The larger but weaker BDC (i.e. following the ± 0.1 kg s^{-3} contours) is characterized by upwelling in the tropics, poleward transport through the stratosphere, and downwelling at high latitudes (particularly in the NH, during the DJF season). Mesospheric transport also features equatorial upwelling and downwelling at high latitudes of the winter hemisphere, though the winter pole is favored.

373 Pressure–weighting the streamfunction highlights the behavior of the middle
374 atmosphere; an example is shown in Fig. 5b. In experiment 1B, during the DJF
375 season, the largest magnitudes occur above 5hPa, with another region of strong
376 upwelling in the equatorial upper troposphere.
377
378 For an in depth comparison of streamfunction values, seven regions are defined.
379 As shown in Fig. 5b, these regions provide good coverage of the features of the
380 BDC. Each of the seven boxes covers a 20° latitude band and spans four model
381 pressure levels. Region 1 is located in the equatorial lower stratosphere (10°S to
382 10°N). Regions 2, 3 and 4 are located in the upper stratosphere; region 3 is
383 centered at the equator, while regions 2 and 4 are located in the SH and NH
384 high latitudes (60° to 80° latitude) respectively. Regions 5, 6 and 7 are located in
385 the mesosphere, region 6 at the equator, and regions 5 and 7 in the SH and NH
386 mid- to high latitudes (40° to 60° latitude).
387
388 Seasonal differences in pressure–weighted streamfunction values generally have
389 the same sign in the equatorial upper troposphere (region 1) as in the
390 mesosphere (regions 5, 6 and 7; not shown). Doubling the background CO_2
391 concentration (for example, 2A–1A or 2C–1B) leads to small changes in
392 streamfunction values in the equatorial UT/LS and larger changes in the upper
393 stratosphere, in the winter hemisphere. These streamfunction changes are
394 positive in the DJF and MAM seasons, but negative in the JJA and SON seasons;
395 streamfunction changes in the NH winter are generally larger than in the SH
396 winter. The difference between the two ozone climatologies (i.e. the difference
397 between experiments 1A and 1B) has little effect on streamfunction values in the
398 troposphere and stratosphere; changes in the mesosphere tend to be smaller
399 than for the difference seen when the background CO_2 concentration is
400 doubled. For the change from the present–day to the future SST climatology,
401 streamfunction values increase (decrease) during the NH (SH) winter. The

magnitude of the changes is larger in the upper troposphere than in the middle atmosphere.

While this initial, qualitative analysis hints at the influence of CO_2, O_3 and forcing from the ocean surface on tropical upwelling and the overturning circulation in the middle atmosphere, a more quantitative approach (which follows) evaluates the relative importance of changes in these three parameters, as well as their variation with altitude and season, on the strength of the BDC under climate change.

5.2 Quantifying Seasonal Differences in the Mean Streamfunction

The impact of changes in ozone, CO_2 and SSTs on the seasonal mean strength of the meridional overturning circulation is assessed quantitatively by grouping together pairs of experiments differing by the same boundary conditions. In Fig. 6, the bars shown in blue represent pairs of experiments which differ only by their O_3 climatology (1980–like – 2000–like); the pink bars represent pairs of experiments which differ only by their background CO_2 concentration (704ppmv – 352ppmv); the green bars represent pairs of experiments which differ only by their SST climatology (future – present–day); the yellow bars represent the climate change signal (2C–1B). Positive values (increased streamfunction) indicate increased transport toward the North Pole, whereas negative values (decreased streamfunction) indicate increased transport toward the South Pole. Values not significantly different from zero indicate that changing a particular parameter has not affected the meridional circulation. Error bars shown in region 5 (in Fig. 6) denote ±1 standard deviation; often, the uncertainties are comparable to the magnitudes of the differences themselves.

Fig. 6 shows pressure–weighed streamfunction differences between pairs of experiments, in the seven atmospheric regions defined in section 5.1, for the DJF

season. Streamfunction values are larger in the idealized future climate scenario (experiment 2C) than in the idealized present–day climate (1B). Furthermore, this figure shows that the relative contribution of the three types of parameter changes is altitude dependent. The SST change dominates the climate change signal in the upper troposphere (region 1) while the CO_2 change dominates in the NH high–latitude upper stratosphere (region 4), and the CO_2 and O_3 changes dominate in the mesosphere (regions 5–7).

Streamfunction differences have a seasonal cycle. Streamfunction differences are generally positive in the DJF season (i.e., increased transport toward the North Pole; see Fig. 6) and negative in the June–July–August (JJA) season (increased transport toward the South Pole; not shown). That is, the strength of the meridional circulation increases in both the NH and SH winter seasons. Generally, differences are positive in the March–April–May (MAM) season and negative in the September–October–November (SON) season, though the magnitudes of these differences are smaller than in the two winter seasons. In regions 2 and 4 (located in the high–latitude upper stratosphere), pressure–weighted streamfunction magnitudes in each of the simulations are small (see Fig. 5b) and the seasonal cycles are much weaker than in other parts of the atmosphere.

5.3 Relationship Between Tropical Upwelling and Polar Ozone

Time–slice simulations with increased CO_2 predict that the polar vortex will strengthen and, assuming the continued presence of anthropogenic chlorine, greater wintertime ozone loss should occur by the mid– to late 21st century (note the differences between 2C and 1B in Fig. 4). The same simulations predict that the strength of the BDC will increase as greenhouse gas concentrations continue to rise and the ozone layer recovers (see Fig. 6). Combining these two

predictions, increased tropical upwelling in early or mid–winter should correlate with a decrease in total column ozone at NH high latitudes in late winter.

For individual time–slice experiments, the correlation between tropical streamfunction and high–latitude total ozone is low, due to the high degree of interannual variability within the 20–year analysis period; García–Herrera et al. (2006) note that relating changes in tropical upwelling and circulation changes at high latitudes is made difficult because of various sources of climate variability, such as the quasi–biennial oscillation (QBO). A more robust relationship between tropical upwelling and polar ozone emerges when the means of each experiment are examined (Fig. 7). As expected, least squares fitting of the eight means yields a negative slope; that is, relative to present–day (experiment 1B), there will be stronger tropical upwelling but lower total ozone near the north pole in March in a future climate (2C)[7]. Though differences between experiments 1B and 2C are statistically significant, the linear regression of January pressure–weighted streamfunction in region 3 as a function of March total ozone at 80°N (Fig. 7) is not.

Correlations of the annual cycles of the pressure–weighted streamfunction between two of the seven atmospheric regions are much higher (generally exceeding 0.90; see Hurwitz, 2008) than for the tropical streamfunction–polar ozone link. That is, increased tropical upwelling corresponds with increased meridional transport in the mesosphere. (Correlations with region 2, which is outside the region of meridional overturning circulation for much of the year, are not statistically significant.) The magnitude of these correlations is generally consistent from experiment to experiment. Thus, although the strength of the BDC is likely to be affected by changes in greenhouse gas concentrations and

[7] Note that this result is a dynamical signature and does not take into account potential changes in ozone chemistry.

other climate forcings, the structure of the circulation pattern itself will remain unchanged.

6 Discussion

This study assessed the roles of three contributors to future stratospheric climate change: increasing CO_2, ozone recovery and generally warmer sea surface temperatures. Stratospheric temperatures, dynamics, ozone and the strength of the Brewer-Dobson circulation were examined in various idealized climate scenarios, using a chemistry–climate model with parameterized ozone chemistry. The 'climate change' signal (2C–1B), the difference from an idealized present–day climate and one predicted for the mid– to late 21st century, corresponded with an increase in polar vortex strength, increased poleward heat fluxes, decreases in stratospheric temperature and a strengthening of the BDC.

In experiments where future SSTs were prescribed (1C-2D; see Table 1), the global mean temperature responses to decreased ozone and increased CO_2 concentrations matched those seen in experiments using present–day SSTs (see Fig. 1). In the stratosphere, the SST–related global mean temperature response was weaker than was the response to doubling CO_2 or to ozone depletion. Nevertheless, the switch from present–day to future SSTs enhanced tropospheric warming and slightly increased global mean temperatures in the lower stratosphere, elevating the tropopause.

A time–lagged linear relation between heat flux and temperature held for all eight time–slice experiments in both winter seasons (see Fig. 2). The NH and SH heat flux–temperature relationships had different slopes, though both showed a positive association between poleward heat fluxes in the upper troposphere

514 and increased polar temperatures in the lower stratosphere. SH dynamics were
515 less sensitive to changes in CO_2, O_3 and SSTs than were NH dynamics.
516
517 As noted by BHP2006, the response to ozone depletion was CO_2–dependent:
518 the NH stratospheric vortex weakened under present–day CO_2 conditions (1B–
519 1A) but strengthened in a doubled–CO_2 atmosphere (2B–2A). This 'flip flop'
520 response was not seen in the four experiments where future SSTs were
521 prescribed. Under future SSTs, prescribed ozone depletion had no significant
522 effect on temperatures, heat fluxes, ozone concentrations or zonal winds at NH
523 high latitudes in winter. This may have resulted from the reduction in
524 baroclinicity in the atmosphere, when SSTs and greenhouse gas concentrations
525 were increased simultaneously.
526
527 A strong anti–correlation between 10hPa zonal wind at 60°N and total ozone at
528 80°N is common to experiments using present–day SSTs (BHP2006) and to the
529 future SST experiments. The lines of best fit were nearly identical. That the
530 relationship between polar vortex strength and polar ozone remained robust,
531 despite large changes in the temperature structure and dynamics of the middle
532 atmosphere, points to the fundamental interdependence of chemistry and
533 climate in the NH polar stratosphere.
534
535 Changes in tropical upwelling and meridional overturning in the middle
536 atmosphere were quantified by examining regional streamfunction variations.
537 In the model experiments, increased tropical upwelling, reduced mid–winter
538 polar ozone and increased polar vortex strength occurred in a climate forced
539 by warmer SSTs and higher greenhouse gas concentrations. The idealized
540 climate change signal (2C–1B) showed a strengthened streamfunction,
541 particularly for the DJF and JJA seasons. This result, therefore, is consistent with
542 previous modeling studies that suggest that the BDC will strengthen in a future

543 climate. The relative contribution of SSTs, O_3 and CO_2 changes to the enhanced
544 circulation in the middle atmosphere was altitude dependent: SST changes
545 played an important role in the tropical upper troposphere (consistent with
546 Garny et al. (2009)), while changes in CO_2 and O_3 dominated the circulation
547 response in the middle atmosphere (see Fig. 6).
548
549 This work predicted no substantial change in the relationship between
550 tropospheric forcing, polar temperature and BDC in a future climate. However,
551 it was not possible to relate climate change–induced increases in tropical
552 upwelling in mid–winter to greater springtime ozone losses at NH high latitudes at
553 statistically significant levels.
554

555 ## Acknowledgements

556 M. M. Hurwitz would like to acknowledge funding from Emmanuel College,
557 Cambridge and from the NASA Postdoctoral Program at Goddard Space Flight
558 Center, administered by Oak Ridge Associated Universities through a contract
559 with NASA. P. Braesicke and J. A. Pyle acknowledge NERC funding through
560 NCAS. The authors thank NCAS–CMS for computational support.
561

561 # References

562

563 Andrews, D. G., J. R. Holton, and C. B. Leovy, 1987: *Middle Atmosphere*
564 *Dynamics*. Academic Press, 489pp.

565

566 Austin, J., and Coauthors, 2003: Uncertainties and assessments of chemistry-
567 climate models of the stratosphere. *Atmos. Chem. Phys.*, **3**, 1–27.

568

569 Austin, J., and F. Li, 2006: On the relationship between the strength of the
570 Brewer–Dobson circulation and the age of stratospheric air. *Geophys. Res. Lett.*,
571 **33**, L17807.

572

573 Braesicke, P., M. M. Hurwitz, and J. A. Pyle, 2006: The Stratospheric response to
574 changes in ozone and carbon dioxide as modelled with a GCM including
575 parameterized stratospheric chemistry. *Meteorol. Z.*, **15**, 343–354.

576

577 Braesicke, P., and J. A. Pyle, 2003: Changing ozone and changing circulation in
578 northern mid–latitudes: Possible feedbacks? *Geophys. Res. Lett.*, **30**, 1059.

579

580 Braesicke, P., and J. A. Pyle, 2004: Sensitivity of dynamics and ozone to different
581 representations of SSTs in the Unified Model. *Q. J. R. Meteorol. Soc.*, **130**, 2033–
582 2045.

583

584 Brewer, A. W., 1949: Evidence for a world circulation provided by the
585 measurements of helium and water vapour distribution in the stratosphere. *Q. J.*
586 *R. Meteorol. Soc.*, **75**, 351–363.

587

588 Butchart, N., and A. A. Scaife, 2001: Removal of chlorofluorocarbons by
589 increased mass exchange between the stratosphere and troposphere in a
590 changing climate. *Nature*, **410**, 799–802.
591
592 Cagnazzo, C., C. Claud, and S. Hare, 2006: Aspects of stratospheric long–term
593 changes induced by ozone depletion. *Climate Dynamics*, **27**, 101–111.
594
595 Cariolle, D., and M. Déqué, 1986: Southern Hemisphere Medium–Scale Waves
596 and Total Ozone Disturbances in a Spectral General Circulation Model. *J.*
597 *Geophys. Res.*, **91**, 10825–10846.
598
599 Chakrabarty, D. K., K. V. Pandya, and N. C. Shah, 2001: Long–term trend of
600 tropopause. *Advances in Space Research*, **28**, 981–986.
601
602 Dhomse, S., M. Weber, I. Wohltmann, M. Rex, and J. P. Burrows, 2006: On the
603 possible causes of recent increases in northern hemispheric total ozone from a
604 statistical analysis of satellite data from 1979 to 2003. *Atmos. Chem. Phys.*, **6**,
605 1165–1180.
606
607 Dobson, G. M. B., 1956: Origin and distribution of the polyatomic molecules in
608 the atmosphere. *Proc. Roy. Soc. A*, **236**, 187–193.
609
610 Eichelberger, S. J., and D. L. Hartmann, 2005: Changes in the strength of the
611 Brewer–Dobson circulation in a simple AGCM. *Geophys. Res. Lett.*, **32**, L15807.
612
613 Engel, A., and Coauthors, 2009: Age of air unchanged within uncertainties over
614 the past 30 years. *Nature Geoscience*, **2**, 28–31.
615

Fomichev, V. I., A. I. Jonsson, J. DeGrandpré, S. R. Beagley, C. McLandress, K. Semeniuk, and T. G. Shepherd, 2007: Response of the middle atmosphere to CO_2 doubling: Results from the Canadian Middle Atmosphere Model. *J. Climate*, **20**, 1121–1144.

García–Herrera, R., N. Calvo, R. R. Garcia, and M. A. Giorgetta, 2006: Propagation of ENSO temperature signals into the middle atmosphere: A comparison of two general circulation models and ERA-40 reanalysis data. *J. Geophys. Res.*, **111**, D06101.

Garny, H., M. Dameris, and A. Stenke, 2009: Impact of prescribed SSTs on climatologies and long–term trends in CCM simulations. *Atmos. Chem. Phys. Discuss.*, **9**, 4489–4524.

Hurwitz, M. M., 2008: *Idealised Numerical Simulations of the Stratospheric Chemistry–Climate System*. PhD Thesis, University of Cambridge, 203pp.

Intergovernmental Panel on Climate Change (IPCC), 2007: *Climate Change 2007: The Scientific Basis: Contribution of Working Group I to the Fourth Assessment Report of the Intergovernmental Panel on Climate Change*, edited by J. T. Houghton et al., Cambridge Univ. Press.

Johns, T. C., and Coauthors, 2003: Anthropogenic climate change for 1860 to 2100 simulated with the HadCM3 model under updated emissions scenarios. *Climate Dynamics*, **20**, 583–612.

Kalnay, E., and Coauthors, 1996: The NCEP/NCAR 40–year reanalysis project. *B. Am. Meteorol. Soc.*, **77**, 437–471.

Li, F., J. Austin, and J. Wilson, 2008: The Strength of the Brewer–Dobson Circulation in a Changing Climate. *J. Climate*, **21**, 40–57.

Lorenz, D. J., and E. T. DeWeaver, 2007: Tropopause height and zonal wind response to global warming in the IPCC scenario integrations. *J. Geophys. Res.*, **112**, D10119.

Manzini, E., B. Steil, C. Bruehl, M A. Giorgetta, and K. Kruger, 2003: A new interactive chemistry–climate model: 2. Sensitivity of the middle atmosphere to ozone depletion and increase in greenhouse gases and implications for recent stratospheric cooling. *J. Geophys. Res.*, **108**, 4429.

Newman, P. A., E. R. Nash, and J. E. Rosenfield, 2001: What controls the temperature of the Arctic stratosphere during the spring? *J. Geophys. Res.*, **106**, 19999–20010.

Oman, L. D., D. W. Waugh, S. Pawson, R. S. Stolarski, and P. A. Newman, 2009: On the influence of anthropogenic forcings on changes in the stratospheric mean age, *J. Geophys. Res.*, **114**, D03105, doi:10.1029/2008JD010378.

Pyle, J. A., P. Braesicke and G. Zeng, 2005: Dynamical variability in the modelling of chemistry–climate interactions. *Faraday Discussions*, **130**, 27–39.

Rex, M., R. J. Salawitch, P. von der Gathen, N. P. R. Harris, M. P. Chipperfield, and B. Naujokat, 2004: Arctic ozone loss and climate change. *Geophys. Res. Lett.*, **31**, L04116.

672 Rex, M., and Coauthors, 2006: Arctic winter 2005: Implications for stratospheric
673 ozone loss and climate change, *Geophys. Res. Lett.*, **33**, L23808,
674 doi:10.1029/2006GL026731.
675
676 Shine, K. P., J. J. Barnett, and W. J. Randel, 2008: Temperature trends derived
677 from Stratospheric Sounding Unit radiances: The effect of increasing CO_2 on the
678 weighting function. *Geophys. Res. Lett.*, **35**, L02710.
679
680 Shine, K. P., and Coauthors, 2003: A comparison of model–simulated trends in
681 stratospheric temperatures. *Q. J. R. Meteorol. Soc.*, **129**, 1565–1588.
682
683 Timmermann, A., J. Oberhuber, A. Bacher, M. Esch, M. Latif, and E. Roeckner,
684 1999: Increased El Niño frequency in a climate model forced by future
685 greenhouse warming. *Nature*, **398**, 694–697.
686
687 Trenberth, K. E., 1997: The Definition of El Niño. *B. Am. Meteorol. Soc.*, **78**, 2771–
688 2777.
689
690 World Meteorological Organisation (WMO), 2007: *Scientific assessment of ozone*
691 *depletion: 2006*, Global Ozone Res. And Monitor. Proj. Rep. 50, Geneva,
692 Switzerland.
693

693 ## Figure Captions

694

695 **Table 1**: Experimental design.

696

697 **Figure 1:** Summary of global and annual mean temperature response for the set
698 of eight time–slice experiments. The left–hand panel shows the ozone–related
699 response (2000–like – 1980–like); the turquoise line shows 1B–1A differences, the
700 yellow line shows 2B–2A differences, the pink line shows 1D–1C differences and
701 the light grey line shows 2D–2C differences. The central panel shows the CO_2–
702 related response ($2xCO_2 - 1xCO_2$); the orange line shows 2A–1A differences, the
703 yellow line shows 2B–1B differences, the dark grey line shows 2C–1C differences
704 and the light grey line shows 2D–1D differences. The right–hand panel shows the
705 SST–related response (future – present–day); the burgundy line shows 1C–1A
706 differences, the pink line shows 1D–1B differences, the dark grey line shows 2C–
707 2A differences and the light grey line shows 2D–2B differences.

708

709 **Figure 2:** Zonal mean meridional mid-latitude heat flux at 100hPa versus polar
710 temperature at 50hPa. For the NH winter, heat fluxes are northward (positive);
711 the scatter plot shows December–January heat fluxes versus January–February
712 temperatures for each year of each experiment. For the SH winter, heat fluxes
713 are southward (negative); the scatter plot shows July–August heat fluxes versus
714 August–September temperatures. Experiment 1A is shown in blue, 1B in
715 turquoise, 2A in orange, 2B in yellow, 1C in burgundy, 1D in pink, 2C in dark grey
716 and 2D in light grey; refer to table 1.

717

718 **Figure 3:** DJF 100hPa heat flux differences between pairs of experiments. The
719 blue bars show heat flux differences due to ozone recovery (1980–like – 2000–
720 like); the pink bars show heat flux differences due to doubling CO_2; the green

721 bars show heat flux differences due to SSTs (future – present–day); the yellow bar
722 shows the climate change signal (2C–1B).
723
724 **Figure 4:** a) Scatter plot of January zonal mean zonal wind versus total ozone for
725 experiments 1A, 1C, 1D, 2C and 2D. b) Scatter plot of the 20–year mean
726 January zonal wind versus total ozone for all eight time–slice experiments. The
727 dotted line shows the mean regression line relating zonal wind to total ozone.
728
729 **Figure 5**: (a) Latitude–height cross–section showing the mean streamfunction for
730 experiment 1B, for the DJF season [$1x10^{-9}$ kg/s^3]. (b) Latitude–height cross–
731 section of the mean pressure–weighted streamfunction (the streamfunction
732 divided by the pressure in hPa) for experiment 1B for the DJF season [$1x10^{-9}$ m/s].
733 The seven numbered boxes identify the atmospheric regions defined in section
734 5.1 of the text.
735
736 **Figure 6**: Pressure–weighted streamfunction differences between pairs of
737 experiments, for seven atmospheric regions, for the DJF season. The spatial
738 organization of the regions is as shown in figure 6b. The four bars for each set of
739 differences denote the DJF, MAM, JJA and SON seasons, respectively. The blue
740 bars represent the response to ozone recovery; the pink bars represent the
741 response to doubled CO_2; the green bars represent the response to increased
742 SSTs; the yellow bars represent the response in the climate change signal (2C–
743 1B). Error bars in region 5 denote ±1 standard deviation.
744
745 **Figure 7**: January streamfunction in region 3 versus March total column ozone at
746 80°N. The colored circles show the 20–year mean for each time–slice
747 experiment; the dashed line shows the line of best fit, fitting the eight mean
748 values.

749 # Figures

Experiment	O_3 Climatology	Background $[CO_2]$ (ppmv)	SST Climatology
1A	1980	352 ($1xCO_2$)	Present–day
1B	2000	352	Present–day
2A	1980	704 ($2xCO_2$)	Present–day
2B	2000	704	Present–day
1C	1980	352	Future
1D	2000	352	Future
2C	1980	704	Future
2D	2000	704	Future

750 **Table 1**: Experimental design.
751

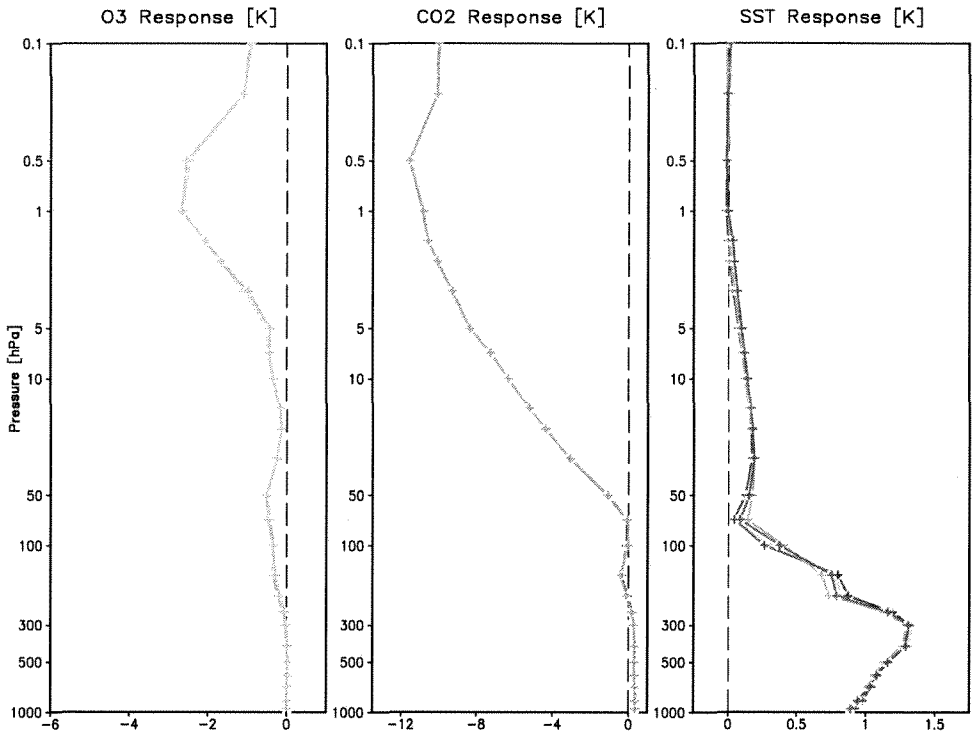

Figure 1: Summary of global and annual mean temperature response for the set of eight time–slice experiments. The left-hand panel shows the ozone–related response (2000–like – 1980–like); the turquoise line shows 1B–1A differences, the yellow line shows 2B–2A differences, the pink line shows 1D–1C differences and the light grey line shows 2D–2C differences. The central panel shows the CO_2–related response ($2xCO_2 - 1xCO_2$); the orange line shows 2A–1A differences, the yellow line shows 2B–1B differences, the dark grey line shows 2C–1C differences and the light grey line shows 2D–1D differences. The right–hand panel shows the SST–related response (future – present–day); the burgundy line shows 1C–1A differences, the pink line shows 1D–1B differences, the dark grey line shows 2C–2A differences and the light grey line shows 2D–2B differences.

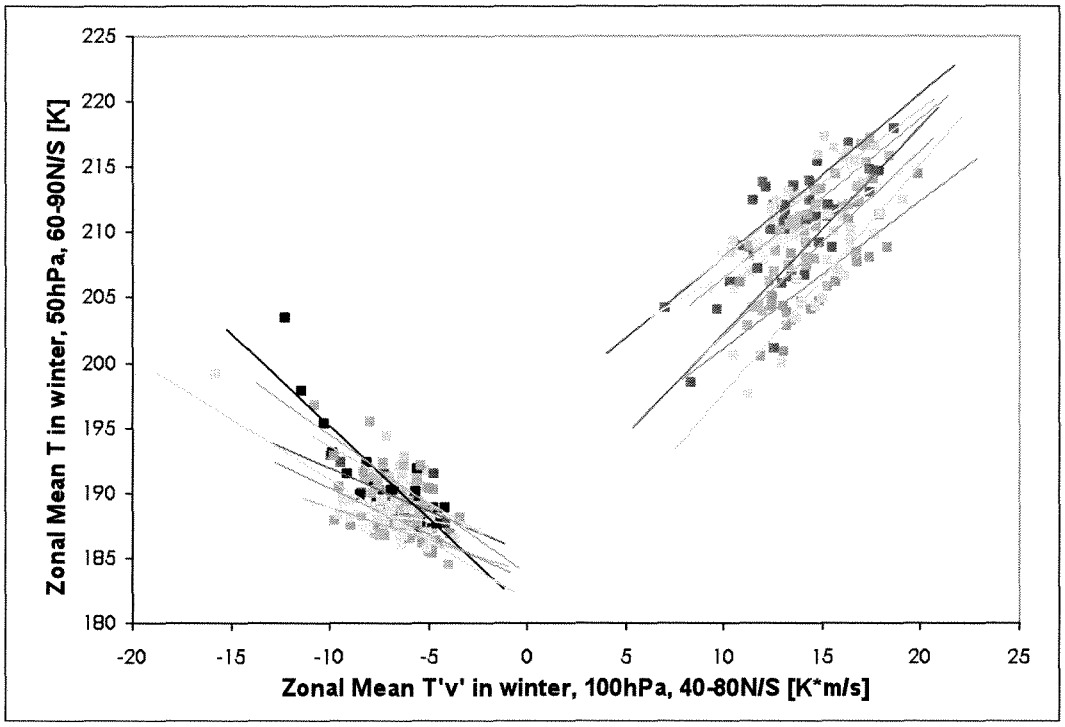

Figure 2: Zonal mean meridional mid-latitude heat flux at 100hPa versus polar temperature at 50hPa. For the NH winter, heat fluxes are northward (positive); the scatter plot shows December–January heat fluxes versus January–February temperatures for each year of each experiment. For the SH winter, heat fluxes are southward (negative); the scatter plot shows July–August heat fluxes versus August–September temperatures. Experiment 1A is shown in blue, 1B in turquoise, 2A in orange, 2B in yellow, 1C in burgundy, 1D in pink, 2C in dark grey and 2D in light grey; refer to table 1.

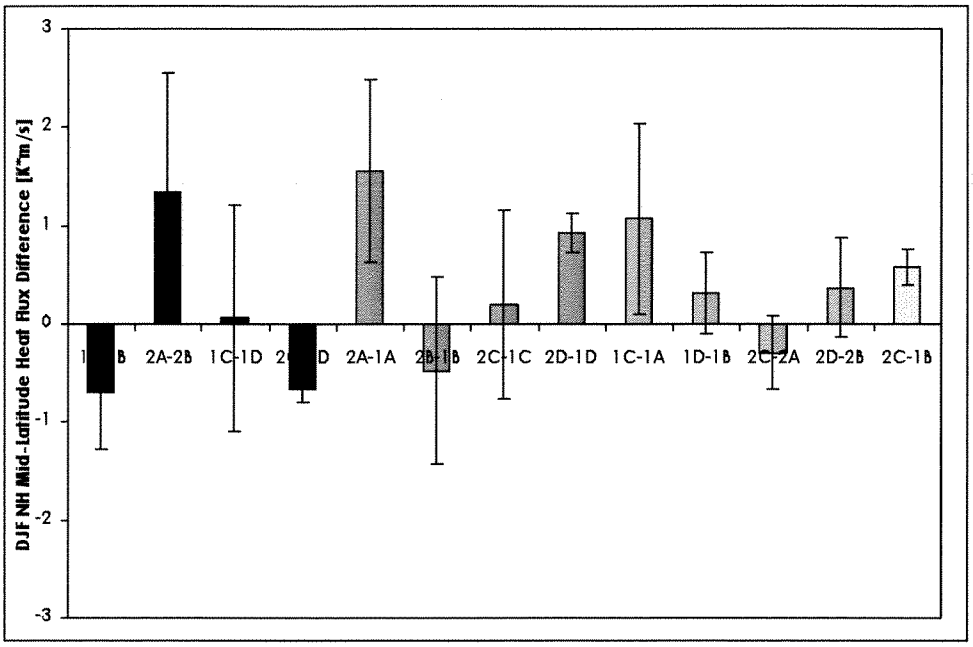

772

773 **Figure 3:** DJF 100hPa heat flux differences between pairs of experiments. The
774 blue bars show heat flux differences due to ozone recovery (1980–like – 2000–
775 like); the pink bars show heat flux differences due to doubling CO_2; the green
776 bars show heat flux differences due to SSTs (future – present–day); the yellow bar
777 shows the climate change signal (2C–1B).
778

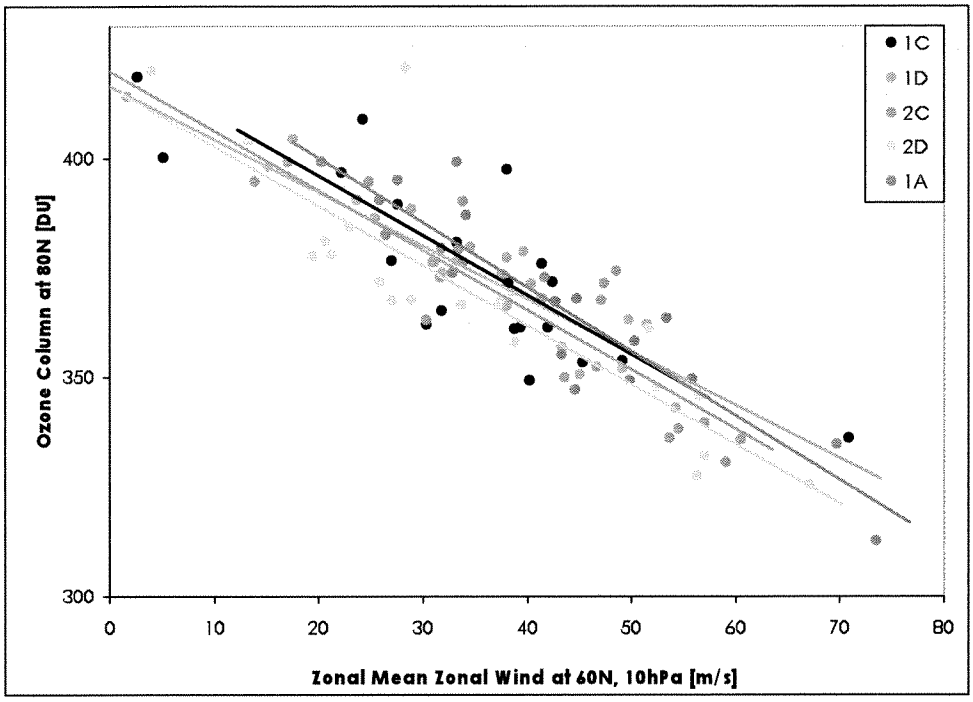

a)

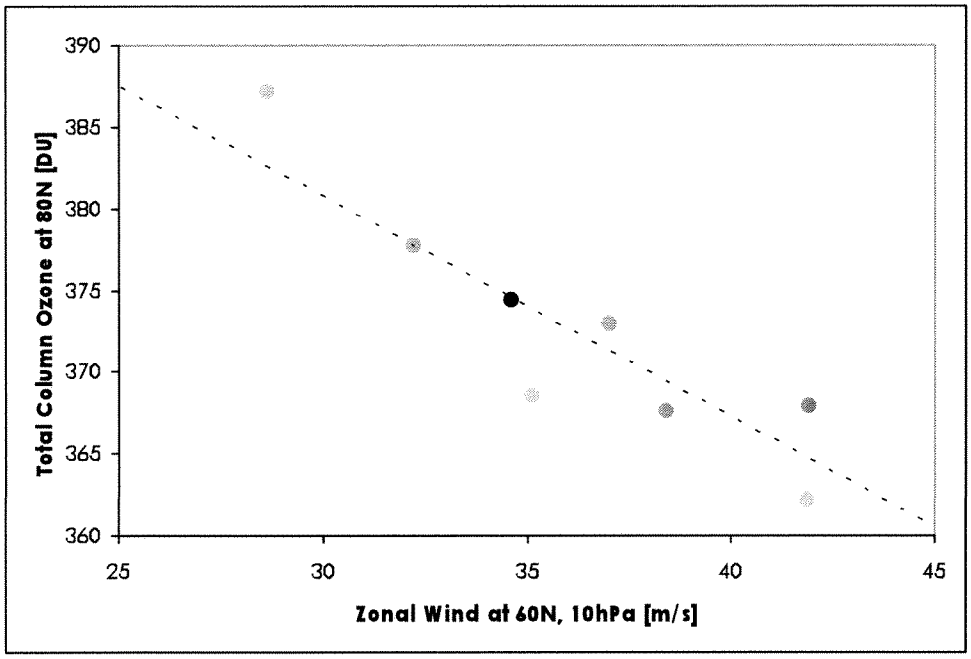

b)

Figure 4: a) Scatter plot of January zonal mean zonal wind versus total ozone for experiments 1A, 1C, 1D, 2C and 2D. b) Scatter plot of the 20–year mean January zonal wind versus total ozone for all eight time–slice experiments. The dotted line shows the mean regression line relating zonal wind to total ozone.

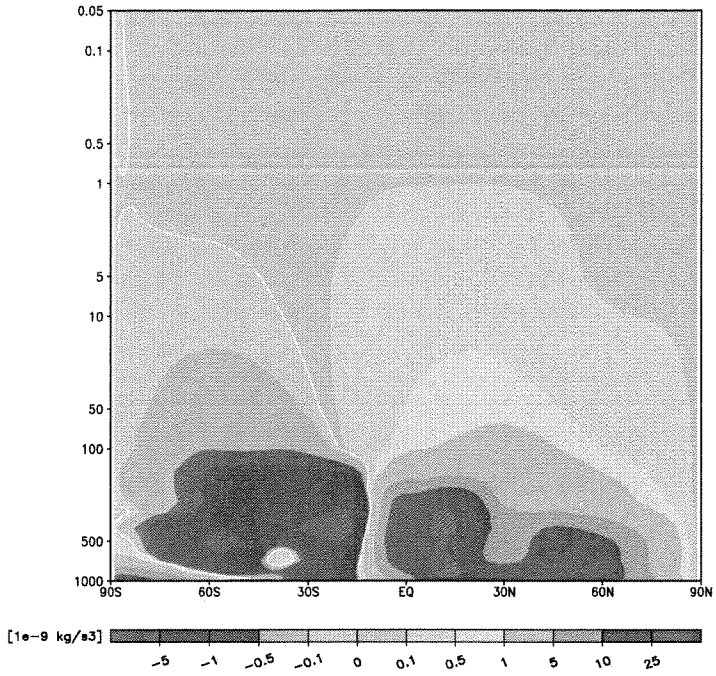

784 a)

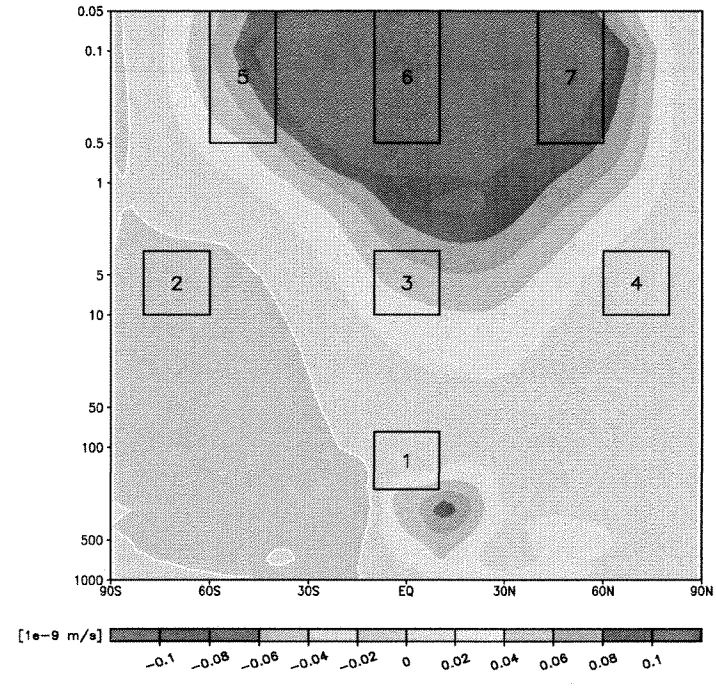

785 b)

786

787 **Figure 5**: (a) Latitude–height cross–section showing the mean streamfunction for
788 experiment 1B, for the DJF season [1x10^{-9} kg/s^3]. (b) Latitude–height cross–

789 section of the mean pressure–weighted streamfunction (the streamfunction
790 divided by the pressure in hPa) for experiment 1B for the DJF season [1×10^{-9} m/s].
791 The seven numbered boxes identify the atmospheric regions defined in section
792 5.1 of the text.

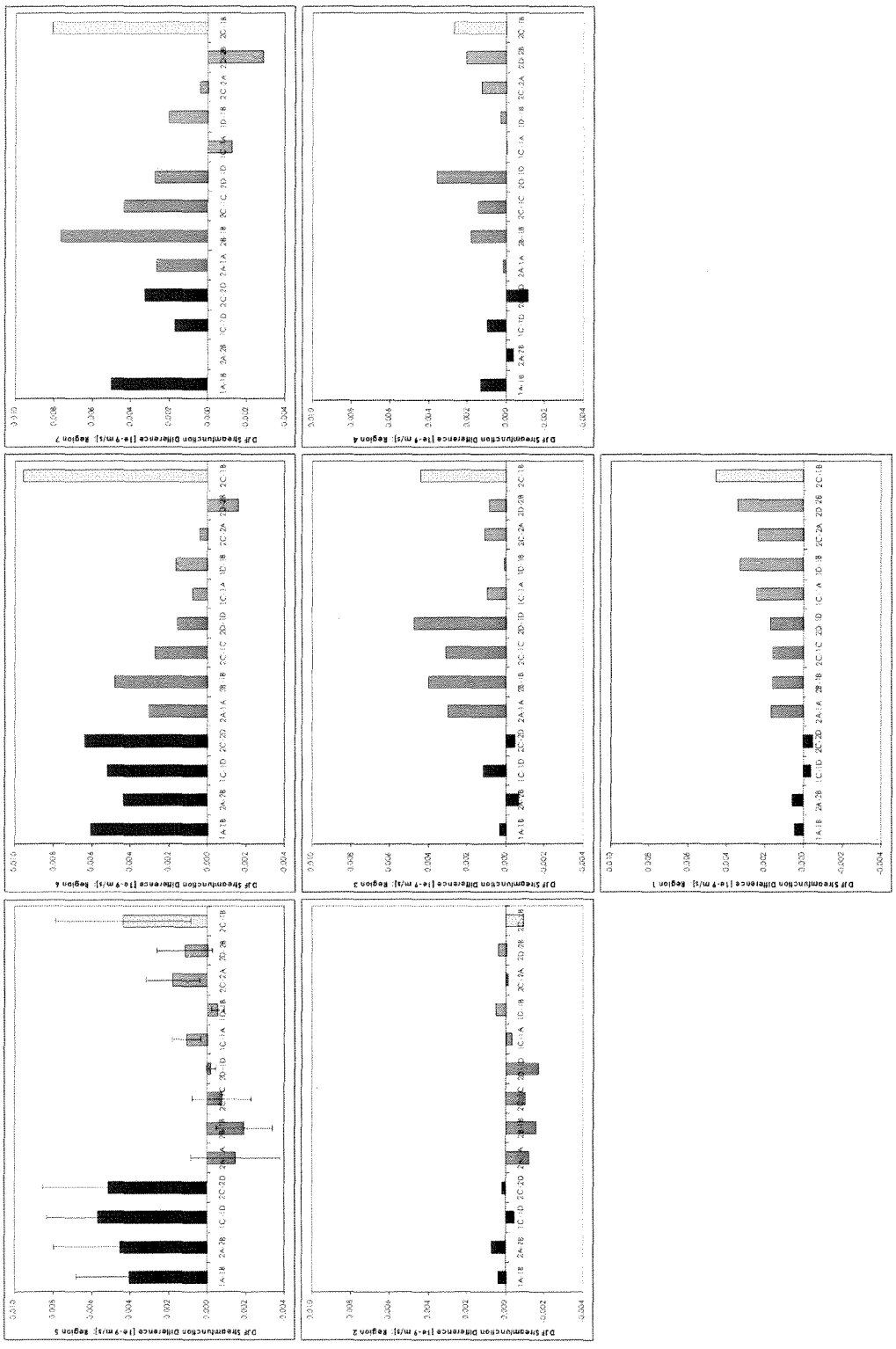
DJF Streamfunction Difference [1e-7 m/s]: Region 1
DJF Streamfunction Difference [1e-7 m/s]: Region 2
DJF Streamfunction Difference [1e-7 m/s]: Region 3
DJF Streamfunction Difference [1e-7 m/s]: Region 4
DJF Streamfunction Difference [1e-7 m/s]: Region 5
DJF Streamfunction Difference [1e-7 m/s]: Region 6
DJF Streamfunction Difference [1e-7 m/s]: Region 7

793

794 **Figure 6**: Pressure–weighted streamfunction differences between pairs of
795 experiments, for seven atmospheric regions, for the DJF season. The spatial
796 organization of the regions is as shown in figure 6b. The four bars for each set of
797 differences denote the DJF, MAM, JJA and SON seasons, respectively. The blue
798 bars represent the response to ozone recovery; the pink bars represent the
799 response to doubled CO_2; the green bars represent the response to increased
800 SSTs; the yellow bars represent the response in the climate change signal (2C–
801 1B). Error bars in region 5 denote ±1 standard deviation.
802

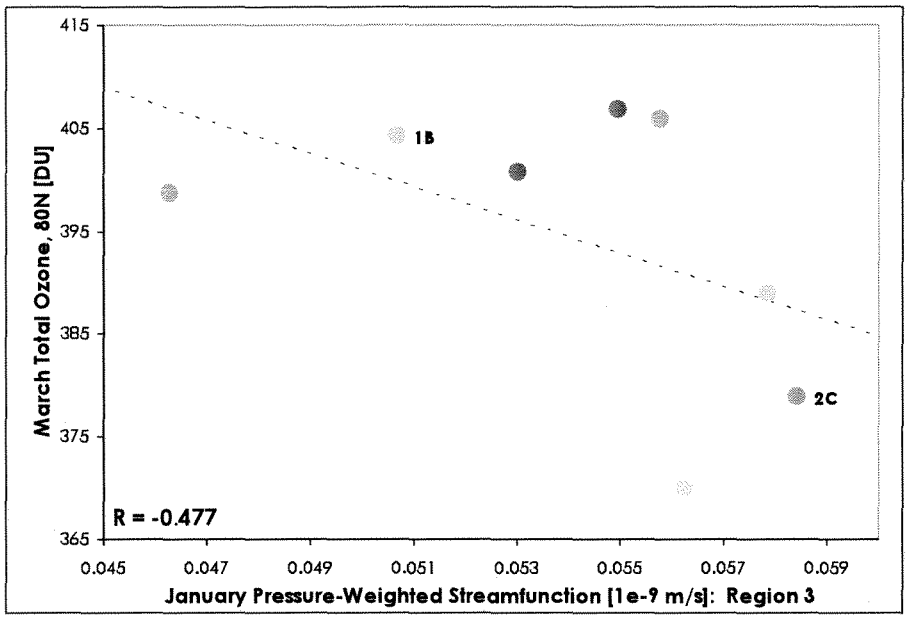

802

803 **Figure 7**: January streamfunction in region 3 versus March total column ozone at
804 80°N. The colored circles show the 20–year mean for each time–slice
805 experiment; the dashed line shows the line of best fit, fitting the eight mean
806 values.